Pergamon

Int. J. Impact Engng, Vol. 17, pp. 409–418, 1995

0734-743X/95 $9.50+0.00

HYPERVELOCITY PENETRATION OF TUNGSTEN SINTER-ALLOY RODS INTO ALUMINUM

V. Hohler, A. J. Stilp and K. Weber

Fraunhofer-Institut für Kurzzeitdynamik, Ernst-Mach-Institut, Impact Physics Division, Eckerstr. 4, 79104 Freiburg, Germany

Summary—The penetration of tungsten sinter-alloy rods having length-to-diameter ratios of L/D = 10 and 12.5 into alumina targets was investigated in the velocity range v_p = 1.25 to 3 km/s. The depth of penetration (DOP) test and the time resolved oberservation using a 600 kV flash X-ray system were applied to assess the protection efficiency of the ceramics. From DOP tests, the residual penetration into a steel backing yields the differential efficiency factor DEF and the mass efficiency factor MEF. DEF increases with v_p; MEF decreases. On the other hand, DEF decreases as ceramic thickness increases; MEF increases and converges to DEF for residual penetration zero. From the time resolved measurements, position and length reduction of the rod during penetration in the ceramics were obtained. The process can be described by Tate's fluid jet model in good approximation. The target resistance parameter R, defined in the modified Bernoulli equation, characterizes the ceramic performance. The average R values are 5.4, 6.1 and 4.8 GPa at impact velocities v_p = 1.7, 2.5 and 3 km/s, respectively, i.e. there is no strong dependence of R on v_p.

NOTATION

CS	Compression strength	R	target material resistance (modified Bernoulli equation)
D	rod diameter	s_K	head position of the rod in the ceramics
DEF	differential efficiency factor	s_H	tail position of the rod in the ceramics
DOP	depth of penetration	t	time
E	Young modulus	u	penetration velocity
h_c	ceramic sheet thickness	v	instantaneous rod velocity
HEL	Hugoniot elastic limit	v_p	impact velocity
HH-RHA	high hard RHA	UTS	ultimate tensile strength
HV	Vickers hardness	WS	tungsten sinter-alloy
l	instantaneous rod length	Y	projectile material flow stress (modified Bernoulli equation)
L_0	launched rod length	α_1/α_2	yaw and pitch angles
L	reduced rod length at impact	δ	elongation
MEF	mass efficiency factor	ρ_c	density of ceramcis
p	semi-infinite penetration in HH-RHA	ρ_p	density of projectile material
p_R	residual penetration in HH-RHA backing	ρ_{st}	density of steel

INTRODUCTION

The terminal ballistic behavior of ceramics has been the subject of many investigations over the past few years. Wilkins et al. [1, 2] did pioneering work by testing thin ceramic plates with an aluminum backing of finite thickness against armor-piercing (AP) projectiles of small L/D-ratio. Later on, the use of ceramics in heavy armor against rod-shaped penetrators became more and more of interest. One of the basic questions has been how to characterize the performance of brittle materials. Hohler and Stilp [3] observed long rods during the penetration of glass with the flash X-ray technique. Based on the material flow of the projectile, which was comparable to that in ductile materials, they proposed, to apply the model of Alekseevskii [4] and of Tate [5] in a first approximation and to use the target resistance parameter R of the modified Bernoulli equation for brittle materials as well.Yaziv et al. [6] defined the differential efficiency factor DEF and the mass efficiency factor MEF. They also found out that the thickness of the backing influences the performance of ceramics. Therefore, in order to get data independent of the backing thickness, Bless et al. [7] introduced the depth of penetration test (DOP) with a semi-infinite backing. Rozenberg and Yeshurun [8] interpreted ceramic efficiency from the static and dynamic (HEL) yield strength for uniaxial strains. Sternberg [9] proposed R values to be in the order of HEL.

The DOP test and the time resolved measurements became the basic test methods. The full significance of the DOP test has been mainly investigated by Woolsey et al. [10, 11], Mellgard et al. [12] and Rozenberg and Tsaliah [13]. Anderson and Morris [14] have shown that the R of alumina concluded from DOP tests is roughly independent of the total ceramic block thickness. Burkett et al. [15], Hauver et al. [16] and Yaziv and Partom [17] have applied both test methods to rod projectiles up to L/D = 20. Among other things, they found a strong influence of the cover plate and the lateral confinement on R. Ernst and Hoog [18] tried to interpret the ceramic performance with static material properties, applying dimensional analysis. Recently, computer code simulation has also been used (Anderson et al. [19]) to better understand long rod penetration in brittle materials.

All this work mentioned above was done in the ordnance velocity range with the exception of the paper by Bless et al. [7]. They concluded from DOP tests up to 2.8 km/s that MEF of alumina decreases with velocity for AP bullets and behaves roughly independent of velocity for Ta rods with L/D = 5. On the other hand, Kozhushko et al. [20] found from penetration velocity measurements of 'elongated copper rods' at 5- 8 km/s an R value for alumina of 26 GPa, which is about 3 to 4 times above HEL. They explained this by the fact that penetration was faster than the crack propagation wave. On the basis of theoretical considerations, Partom and Littlefield [21] postulate an increase of R with velocity in the range up to 3 km/s.

Velocities above the ordnance range become more and more important for long rod penetrators. Therefore, the purpose of this paper is to study the influence of velocity upon penetration performance of tungsten sinter-alloy rods (WS) in the case of alumina targets. The velocity range covers 1.25 to 3 km/s. In addition, the thickness of the ceramic tiles and their lateral dimensions, as well as their lateral confinement, were varied. DOP tests and time resolved measurements using a 600 kV flash X-ray system were applied.

EXPERIMENTS

Tests were run with WS rods at four impact velocities v_p = 1.25, 1.7, 2.5 and 3 km/s. Two different WS qualities were used. The rods are cylindrical in shape with L/D-ratios of 10 and 12.5. They are launched up to 1.7 km/s by a powder gun and up to 3 km/s by a two-stage light gas gun. The original rod length L_0 is reduced at higher velocities to length L by plastic deformation during acceleration. So L means the actual rod length in the moment of impact. The properties of the WS materials and the geometrical parameters of the rods are summarized in Table 1.

Fig. 1 shows the DOP target arrangement used up to $v_p \leq 1.7$ km/s. The total ceramic block thickness h_c is varied at v_p = const. by fitting different numbers of 20 mm thick Al_2O_3 tiles up to residual penetration $p_R = 0$ in the semi-infinite high hard armor steel backing (HH-RHA, material properties see Table 1). The lateral dimensions of the tiles are 100, 150 and 180 mm. The ceramic block is laterally confined by 20 mm and in front by 10 mm mild steel plates. The front plate has a 30 mm hole for the rod

impact. A 1.5 mm rubber foil is inserted in between the front cover plate and ceramics for stress dampening. Pitch and yaw angles are measured by flash X-ray systems during impact.

In the case of observing the penetrator inside the ceramics, the lateral dimensions of the ceramics and the use of confinement are restricted. The available 600 kV flash X-ray system delivers pictures of acceptable quality for maximal lateral tile dimensions of 100 mm. Therefore the target arrangement of Fig. 2 was used for these measurements, performed at $v_p \geq 1.7$ km/s. Now the ceramic block is only partly confined because of the 50 mm window for the flash X-ray observation. The ceramic block is built of 20 mm tiles at 1.7 km/s and of 10 mm tiles at 2.5 and 3 km/s; one test was done with 5 mm and one with 20 mm tiles at 3 km/s. The measured parameters are defined in Fig. 3. Time is recorded by triggering the 180 and 600 kV systems with a short circuit trigger foil and by counting the time between the two flashes. The moment of impact (t = 0) was determined from the 180 kV flash X-ray picture. The accuracy of the penetration time t is ± 0.15 μs. The uncertainties of l, s_K and s_H are ± 0.1 mm and ± 0.2 mm, respectively.

All ceramic tiles are square in shape and plane grinded. They are glued together, to the backing, and to the confinement with a two-component epoxy adhesive.

The manufacturer of the Al_2O_3 tiles was Hoechst CeramTec, Germany. All tiles are produced according to the same production procedure, characterized by the trade name A1898. This guarantees a good consistency of the material properties, given in Table 1.

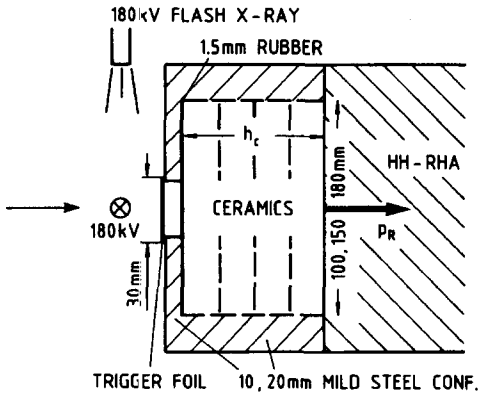

FIG. 1. DOP test arrangement applied at 1.25 and 1.7 km/s.

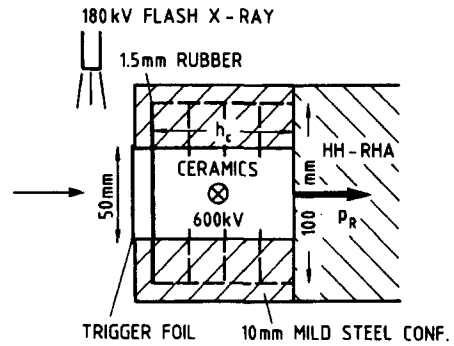

FIG. 2. Arrangement for DOP- and time resolved tests used at $v_p \geq 1.7$ km/s.

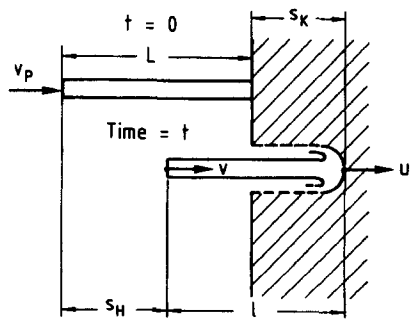

FIG. 3. Definition of parameters for time resolved measurements.

TABLE 1. PARAMETERS OF ROD PROJECTILES AND TARGET MATERIALS (*NAHME [22])

Projectile Material	v_p [km/s]	L_0 [mm]	L_0/D	L [mm]	ρ_p [g/cm^3]	UTS [GPa]	HV [GPa]	δ [%]
WS_1	1.25/1.7	72.5	12.5	72.5	17.6	1.2 ± 0.02	4.2 ± 0.1	10 ± 1
WS_2	2.5/3.0	50	10	49.9/49.5	17.6	1.49 ± 0.015	5.35 ± 0.1	8.8 ± 2

Steel backing	ρ_{St} [g/cm^3]	UTS [GPa]	HV [GPa]
HH-RHA	7.85	1.45 ± 0.1	4.4 ± 0.2

Ceramics	ρ_c [g/cm^3]	CS [GPa]	HV [GPa]	grain size [μm]	E [GPa]	HEL [GPa]	Poisson ratio
Al_2O_3	3.8	4.0	21	6 - 12	360	5.3 - 7.5 *	0.24 - 0.26

RESULTS

The experimental data are summarized in Table 2. Experiments with Nos. ≤ 2019 are DOP tests (Fig. 1). Experiments with Nos. ≥ 7349 are DOP tests in combination with time resolved measurements (Fig. 2). Beside the test Nos., the symbols used in the diagrams are given. Since v_p in the experiments shows a certain spread s_K, s_H, l, u and v have been corrected to v_p = 1.7, 2.5 and 3.0 km/s according to, e.g., $s_K(v_{p1}) = (v_{p1}/v_{p2}) \cdot s_K(v_{p2})$. No adjustment of time t was performed. u and v means average velocities with $u = s_K/t$ and $v = s_H/t$. R has been calculated on the basis of the modified Bernoulli equation and means an average value referring to penetration time t. Y = 2 and 2.3 GPa were used for WS_1 and WS_2, respectively.

The DOP test reveals the residual penetration p_R, the semi-infinite penetration p and the differential and mass efficiency factors with

$$DEF = \frac{(p - p_R)\rho_{st}}{\rho_c h_c} \qquad MEF = \frac{p\,\rho_{st}}{\rho_c h_c + p_R \rho_{st}}$$

p_R/p, DEF and MEF are plotted versus $\rho_c h_c/L$ in Figs. 4, 5 and 6. The normalization by L is needed because of the two different L/D-ratios used in the experiments. The data in these three diagrams refer to the experimental impact velocity v_p, i.e., p has been corrected according to the data in Table 3. Since p_R/p, DEF and MEF depend only slightly on v_p, the corrected data in the diagrams are also valid in good approximation at the four central velocities 1.25 km/s, etc.

The main result of Fig. 4 implies that p_R/p increases with v_p. No remarkable change of the curve trace is observed dependent upon v_p. The points marked by an arrow mean extrapolation to $p_R/p = 0$. The corresponding h_c value is some kind of semi-infinite penetration in Al_2O_3. At v_p = 1.7 km/s the influence of the two different confinements (see Figs. 1 and 2) and of the different lateral tile dimensions can be seen. Both confinements behave alike for lateral tile dimensions of 100 mm in the total h_c range. On the other hand, p_R is a little less for lateral tile dimensions ≥ 150 mm for $\rho_c h_c/L > 3.25$ ($h_c > 60$ mm). Therefore, two extrapolated values are given at 1.7 km/s. The time to penetrate 60 mm ceramics is in the order of t = 65 μs (s. Table 2). According to Anderson and Morris [14], edge effects play a role if $t > 2t^*$, where t^* is the average time of the longitudinal and shear waves needed to propagate to the lateral target edge and back to the trajectory. In the case of 100 mm lateral tile dimensions with a 10 - 20 mm confinement, t^* is about 18 - 22 μs. So it may be concluded that for the test arrangement applied here, edge effects play a role if $t > 3\,t^*$.

The targets built up by 5, 10 or 20 mm thick tiles show a negligible influence of the tile thickness on p_R/p at 3 km/s (see Table 2, Nos. 7839, 7843, 7844).

The general tendencies of DEF dependent upon v_p and h_c are indicated in Fig. 5. For v_p = const., DEF decreases with h_c and converges at $p_R = 0$ versus MEF, which had already been observed by Ernst and Hoog [18] in the ordnance velocity range. Furthermore DEF grows with v_p. This behavior is very interesting and may be expected. However the curves become flatter at higher velocities and come closer together, i.e., the increase of DEF with v_p is reduced at higher velocities, nearly disappears from 2.5 to 3 km/s and is strongly dependent upon h_c.

TABLE 2. LIST OF DATA

No.	Symbol	No. of cer. tiles of thickness			h_c	lat tile dim.	v_p	α_1/α_2	$p_R(v_p)$
		5	10	20 mm	[mm]	[mm]	[m/s]	[°]	[mm]
2017	•			1	19.8	180	1246	1.0/<1.0	17.5
2018	•			2	39.6	180	1246	1.0/<1.0	5.0
2019	•			3	59.8	180	1252	0.0/<1.0	0.0
2002	o			1	20.2	100	1705	0.3/<1.0	42.6
2003	o			2	40.1	100	1709	1.8/<1.0	28.9
2004	o			3	61.1	100	1702	1.5/<1.0	16.7
2000	o			4	81.4	100	1705	4.8/<1.0	4.2
2014	Δ			1	20.0	150	1717	0.8/<1.0	43.4
2011	Δ			2	40.0	150	1721	<0.5/<1.0	31.7
2012	Δ			3	60.0	150	1717	0.8/<1.0	14.7
2013	Δ			4	80.0	150	1716	1.0/<1.0	2.8
1986	∇			1	19.9	180	1710	0.3/<1.0	44.6
1985	∇			2	39.5	180	1711	0.5/<1.0	30.2
1984	∇			3	59.6	180	1698	1.0/<1.0	15.2
1983	∇			4	79.0	180	1708	1.0/<1.0	2.2
7393	□			2	40.6	100	1711	0.7/<1.0	29.7
7349	□		1	2	51.0	100	1691	0.8/<1.0	19.4
7394	□			3	60.0	100	1706	0.5/<1.0	14.5
7395	□			4	80.7	100	1710	≤1.0/<1.0	4.6
7899	■		1		10	100	2552	0.2/1.7	60.2
7900	■		2		20	100	2522	1.0/6.4	50.7
7901	■		3		30	100	2537	0.1/<0.5	39.1
7902	■		5		50	100	2550	0.1/1.9	23.9
7903	■		7		70	100	2516	0.5/0.2	10.2
7896	+		1		10	100	3024	<2.0/3.1	66.8
7905	+		1		10	100	3023	<1.0/4.8	67.0
7907	+		1		10	100	2994	0.2/1.4	68.0
7836	+		2		20.5	100	2984	2.0/<1.0	58.1
7847	+		2		19.9	100	3002	0.5/1.5	58.3
7848	+		2		19.6	100	2968	3.0/1.6	58.8
7904	+		3		30	100	3025	0.5/0.2	50.0
7845	+		3		30.8	100	3000	0.0/3.0	50.2
7837	+		4		40.8	100	2991	0.3/<1.0	38.6
7840	+		4		41.1	100	3000	0.2/<1.0	40.1
7849	+		4		40.4	100	2995	4.8/0.2	41.3
7838	+		6		62.0	100	3037	0.3/<1.0	21.6
7850	+		7		69.8	100	2980	<1.0/<1.0	18.7
7839	+		8		82.0	100	3003	<1.0/<1.0	7.5
7843	x			4	81.1	100	2998	<1.0/<1.0	8.8
7844	◊	15			80.8	100	2995	<1.0/0.0	9.0
7851	+		10		101.2	100	2964	<1.0/0.1	0
7852	+		10		100.5	100	2963	<1/1.5	0

TABLE 2. LIST OF DATA (CONTINUED)

No.	t	s_K	l	u	R
	[μs]	[mm]	[mm]	[m/s]	[GPa]
7393	21.2	20.5	56.8	961	5.1
7349	26.0	24.4	52.7	943	5.4
7394	53.0	47.6	30.5	895	6.0
7395	81.1	72.4	13.2	888	5.1
7899	5.0	7.8	45.1	1560	5.5
7900	10.6	16.4	39.9	1547	5.7
7901	17.5	26.3	32.1	1503	6.7
7902	29.7	44.9	21.2	1511	6.3
7903	31.5	47.2	19.3	1498	6.4
7907	4.5	8.9	44.9	1973	4.2
7847	3.0	5.9	46.3	1967	4.3
7848	4.2	8.2	45.1	1952	4.7
7904	14.7	28.6	34.4	1945	4.7
7845	12.7	25.0	36.3	1969	4.3
7849	19.3	37.6	30.9	1948	4.8
7850	32.9	63.1	14.8	1918	5.1
7843	39.0	72.2	7.9	1852	5.8
7844	38.7	73.4	8.4	1897	5.4
7852	39.3	73.9	8.9	1881	4.9

TABLE 4. SEMI-INFINITE PENETRATION p AND VELOCITY DEPENDENCE OF p IN THE BACKING STEEL HH-RHA

	v_p [km/s]	p [mm]	L [mm]	dp/dv_p [10^{-2} mm/(m/s)]
WS_1	1.25	33.0	72.5	6.27
WS_1	1.7	62.4	72.5	6.27
WS_2	2.5	68.3	49.9	2.13
WS_2	3.0	76.3	49.5	1.16

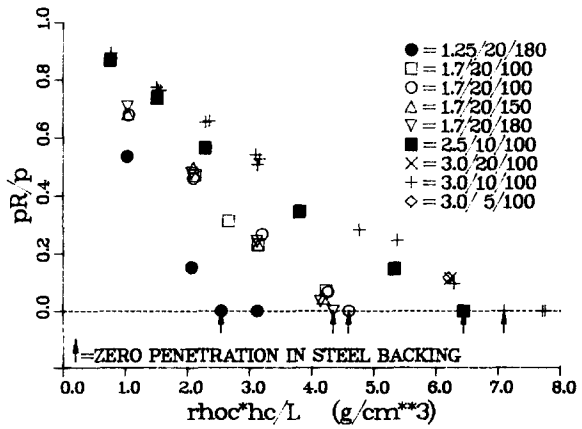

FIG. 4. Residual penetration p_R versus ceramic block thickness h_c. The arrow symbols mark extrapolated values h_c ($p_R = 0$). 1.25 / 20 / 180 etc. means v_p = 1.25 km/s / 20 mm tile thickness / 180 mm lateral tile dimension.

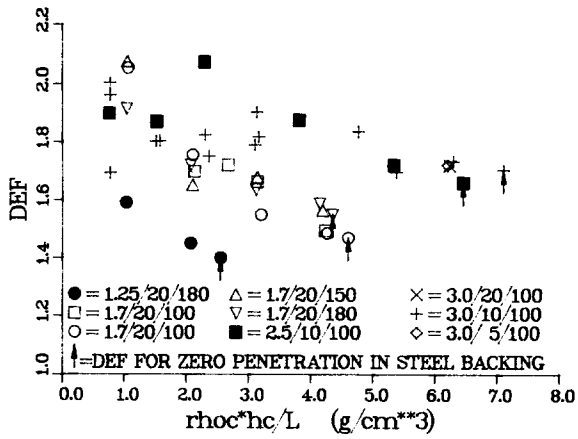

FIG. 5. Differential efficiency factor DEF versus ceramic block thickness h_c.

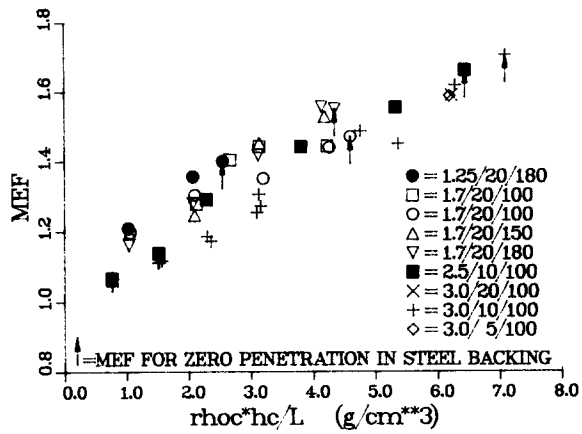

FIG. 6. Mass efficiency factor MEF versus ceramic block thickness h_c.

The MEF parameter gives the best quantitative assessment about the protection improvement of a real target using ceramics. The MEF data are plotted in Fig. 6. MEF increases with h_c and achieves its maximum at $p_R = 0$. Furthermore, MEF goes down with v_p for h_c = const. So an increase of MEF at a higher velocity v_{p2} becomes possible only since h_c (v_{p2}) can be thicker than h_c (v_{p1}), if $v_{p2} > v_{p1}$.

Fig. 7 shows some examples of flash X-ray pictures of the penetration process taken with the 600-kV system. No. 7394 is taken from a rod with caliber 5.8 mm, the others from rods with caliber 5 mm. For a better quantitative comparison, picture No. 7394 is reduced by a factor 5/5.8. One may see that the rods behave according to the fluid jet model. There are some discontinuities of the material flow at the interfaces between the tiles. This indicates an influence of the interfaces on the process. On the other hand, such an influence on p_R, s_K or l etc. (see Table 2 and Fig. 7, Nos. 7839, 7843, 7844, 7852) cannot be observed in the tests made at 3 km/s with 5, 10 or 20 mm thick tiles. Therefore a general conclusion cannot be made that tile thickness has a negligible influence.

The R data in Table 2 depend on t in the same manner at all velocities. R increases with t during early penetration, achieves a plateau and decreases slightly during late penetration. This behavior had already been observed and explained by Hauver et al. [16] at ordnance velocities. The reduction of R during early penetration occurs only in tests without a cover plate, as done here and is caused by the impact damage. The small reduction during late penetration is explained by the predestruction of the ceramics in front of the rod. The velocity dependence of R is relatively small. The average R data are 5.4, 6.1 and 4.8 GPa at

1.7, 2.5 and 3.0 km/s. R is in the order of HEL (see Table 1, Sternberg [9]). No increase of R up to 3.0 km/s can be observed, as was expected by Partom and Littlefield [21].

The data for s_K, s_H and l are plotted in Figs. 8 and 9 versus normalized time $t \cdot v_p/L$ and normalized head position $\rho_c s_K/L$. The curves were calculated on the basis of Tate's model (Tate [5]), using the average R values for Al_2O_3 and Y = 2 and 2.3 GPa for WS_1 and WS_2, respectively. The calculation was done within the limits v_p and v', where $v' = (2(R-Y)\rho_p)^{1/2}$. Now, according to Anderson et al. [19], the R value of HH-RHA is 5 GPa. Therefore v' is calculated using the R value 5 GPa of HH-RHA at 3 km/s and the average R values 5.4 and 6.1 GPa of Al_2O_3 at 1.7 and 2.5 km/s, respectively. There is good agreement between experiment and calculation. Some deviations occur during late penetration. It is interesting that the simple one-dimensional model delivers a good description of the process. However this fact should not be overinterpreted. There is a need to develop improved theoretical models. Nevertheless, the R values determined from time resolved measurements can be considered to be characteristic quantities in describing the protection performance of brittle materials also.

Fig. 10 shows the average rod erosion $(L-l)/s_K$ versus s_K. This erosion decreases with v_p and behaves according to R, i.e., the erosion increases during early penetration up to a plateau and slows down slightly during late penetration. The decrease during late penetration depends upon v_p and nearly disappears at 3 km/s.

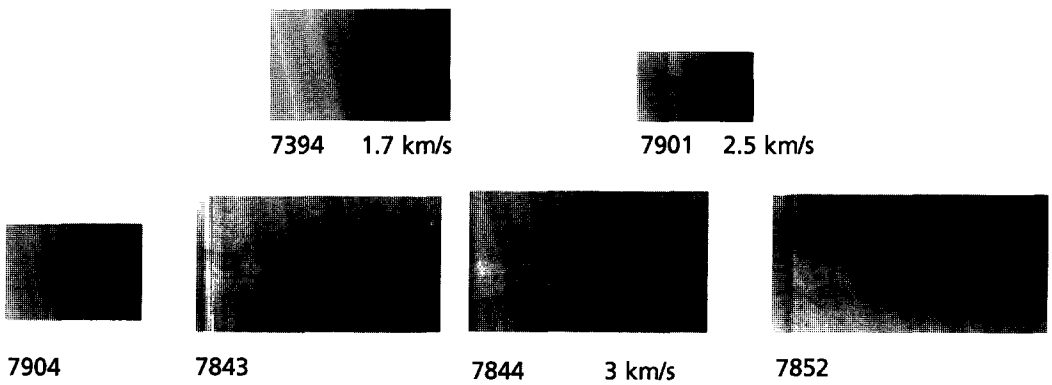

FIG. 7. Flash X-ray pictures taken from the penetration process.

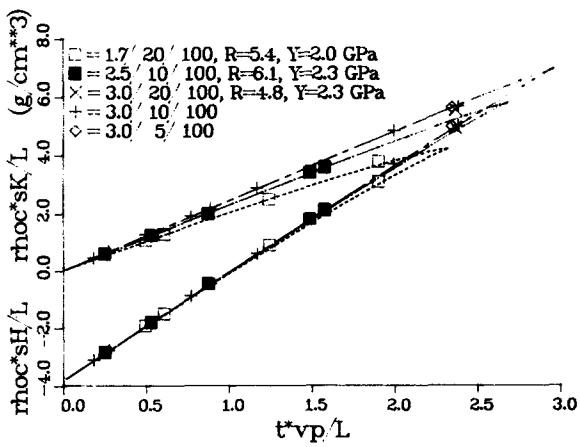

FIG. 8. Front and tail positions s_K and s_H of the penetrating rod versus time t. The curves are calculated according to Tate.

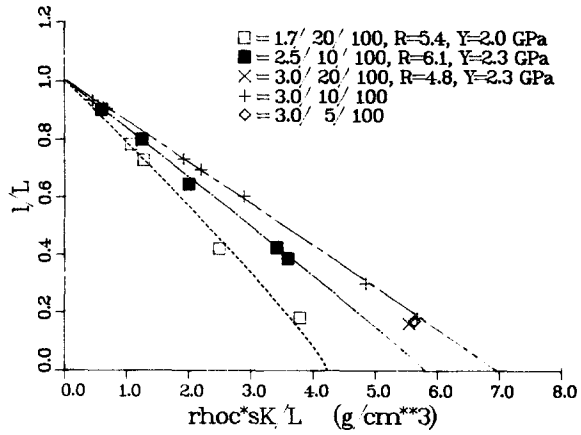

FIG. 9. Residual length l versus head position s_K. The curves are calculated.

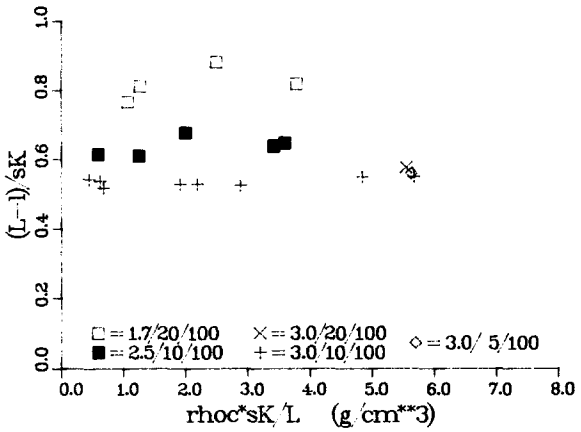

FIG. 10. Average rod erosion (L-l) versus head position s_K.

CONCLUSIONS

The protection efficiency of alumina ceramics against long rod projectiles has been investigated up to an impact velocity of 3 km/s. DOP tests and time resolved measurements were performed. It can be shown that Tate's fluid jet model also describes the penetration process above ordnance velocities in good approximation. The resistance R defined in the modified Bernoulli equation is a good parameter to characterize the protection efficiency of the ceramics. R shows no remarkable dependence on the impact velocity. Despite the good approximation achieved by Tate's model, there is a need to develop an improved description of the process, taking into account, e.g. crack propagation effects.

REFERENCES

1. M. L. Wilkins, C. F. Cline and C. A. Honodel, Fourth progress report of light armor program. *Lawrence Radiation Lab. Rept. UCRL-50694* (1969).
2. M. L. Wilkins, R. L. Landingham and C. A. Honodel, Fifth progress report of light armor program. *Lawrence Radiation Lab. Rept. UCRL-50980* (1971).

3. V. Hohler and A. J. Stilp, Visualization of the penetration process of rods into glass and armor steel targets by means of flash X-ray photographs. *Proc. 35th ARA Meeting*, Meppen, Germany (1984).
4. V. P. Alekseevskii, Penetration of a rod into a target at high velocity. *Fizika Goreniya Vzryra*, **2**, 99 (1966).
5. A. Tate, A theory for the deceleration of long rods after impact. *J. Mech. Phys. Solids*, **15**, 387 (1967).
6. D. Yaziv, G. Rosenberg and Y. Partom, Differential ballistic efficiency of appliqué armor. *Proc. 9th Int. Symp. Ballistics*, Shrivenham, UK (1986).
7. S. J. Bless, Z. Rozenberg and B. Yoon, Hypervelocity penetration of ceramics. *Int. J. Impact Engng.*, **5**, 165 (1987).
8. Z. Rozenberg and Y. Yeshurun, The relation between ballistic efficiency and compressiv strength of ceramic tiles. *Int. J. Impact Engng.*, **7**, 357 (1988).
9. J. Sternberg, Material properties determining the resistance of ceramics to high velocity penetration. *J. Appl. Phys.*, **65**, 3417 (1989).
10. P. Woolsey, St. Mariano and D. Kokidko, Alternative test methodology for ballistic performance ranking of armor ceramics. *Proc. 5th Annual TACOM Armor Coordinating Conference*, Monterey, CA, USA (1989).
11. P. Woolsey, Ceramic materials screening by residual penetration ballistic testing. *Proc. 13th Int. Symp. Ballistics*, Stockholm, Sweden (1992).
12. I. Mellgard, L. Holmberg and L. G. Olsson, An experimental method to compare the ballistic efficiencies of different ceramics against long rod projectiles. *Proc. 11th Int. Symp. Ballistics*, Brussels, Belgium (1989).
13. Z. Rozenberg and J. Tsaliah, Applying Tate's model for the interaction of long rod projectiles with ceramic targets. *Int. J. Impact Engng.*, **9**, 247 (1990).
14. Ch. E. Anderson and B. L. Morris, The ballistic performance of confined Al_2O_3 ceramic tiles. *Int. J. Impact Engng.*, **12**, 167 (1991).
15. M. W. Burkett, G. E. Cort, R. B. Parker, A. D. Rollett and S. R. Skaggs, Ballistic performance evaluation of 90 wt % Al_2O_3 against a subscale kinetic energy long rod penetrator. *Proc. 13th Int. Symp. Ballistics*, Stockholm, Sweden (1992).
16. G. E. Hauver, P. H. Netherwood, R. F. Benck, W. A. Gooch, W. J. Perciballi and M. S. Burkins, Variation of target resistance during long rod penetration into ceramics. *Proc. 13th Int. Symp. Ballistics*, Stockholm, Sweden (1992).
17. D. Yaziv and Y. Partom, The ballistic efficiency of thick alumina targets against long rod penetrators. *Proc.14th Int. Symp. Ballistics*, Quebec, Canada (1993).
18. H. J. Ernst and K. Hoog, Protective power of several ceramics, correlated to some static material parameters. *Proc. 13th Int. Symp. Ballistics*, Stockholm, Sweden (1992).
19. Ch. E. Anderson, V. Hohler, J. D. Walker and A. J. Stilp, Penetration of long rods into steel and glass target: Experiments and computations. *Proc. 14th Int. Symp. Ballistics*, Quebec, Canada (1993).
20. A. A. Kozhushko, I. I. Rykova and A. B. Sinani, Resistance of ceramics to penetration at impact velocities above 5 km/s. *J. de Physique IV* (Colloque C3, suppl. au J. de Physique III), **1**, 117 (1991).
21. Y. Partom and D. L. Littlefield, Dependence of ceramic armor resistance on projectile velocity. *Proc. 14th Int. Symp. Ballistics*, Quebec, Canada (1993).
22. H. Nahme, Ernst-Mach-Institut. Private communication (1994).